Heliyon 10 (2024) e38151

Contents lists available at ScienceDirect

Heliyon

journal homepage: www.cell.com/heliyon

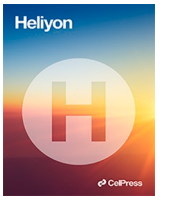

Research article

Cigarette smoke extract induces ferroptosis in human retinal pigment epithelial cells

Long Zhao [1], Ping Wu [1], Jing Lu, Yuxia He, Qinxin Shu, Fuying Pan, Hao Xie, Xing Wang, Huan Ju, Yong Du [**], Hui Peng [*]

The First Affiliated Hospital of Chongqing Medical University, Chongqing Key Laboratory of Ophthalmology, Chongqing Eye Institute, Chongqing Branch (Municipality Division) of National Clinical Research Center for Ocular Diseases, Chongqing, China

ARTICLE INFO

Keywords:
Ferroptosis
Cigarette smoke extract
Retinal pigment epithelium
Age-related macular degeneration

ABSTRACT

Background: Age-related macular degeneration (AMD) is a common blindness diseases. Retinal pigment epithelium (RPE) dysfunction due to smoking is an essential environmental factor in the pathogenesis of AMD. Ferroptosis is a novel type of iron-dependent programmed cell death (PCD). However, the relationship between cigarette smoke extract (CSE)-induced RPE damage and ferroptosis remains unclear.

Methods: In our study, we extracted CSE using a modified device to explore the optimal concentration of CSE, and observed the expression of proteins and molecules after CSE exposure for ARPE-19 cells by protein immunoblotting and assay kits for iron ions and mitochondrial membrane potential (MMP). At the same time, CSE was injected into the vitreous cavity of mice with a microsyringe for AMD modeling to observe the morphology of the retina-RPE-choroid complex and the differences expression of proteins. In addition, the protective effects of ferroptosis inhibitors on CSE-induced RPE cell damage were also investigated by in vivo and in vitro experiments.

Results: In this study, we observed that CSE induced cellular damage in a human retinal pigment epithelial cell line (ARPE-19), resulting in ferrous ion (Fe^{2+}) accumulation, an increas in reactive oxygen species (ROS) and lipid peroxidation (LP), a reduction in GSH levels, and the inhibition of Gpx4 expression. In addition, transmission electron microscopy (TEM) of in vivo and in vitro samples showed that after exposure to CSE, the mitochondria of RPE cells were wrinkled, the membrane density was increased, and the number of cristae decreased or cristae were not observed.

Conclusions: The results of this study indicate that the ferroptosis inhibitors ferrostatin-1 (Fer-1) and liproxstatin-1 (Lip-1) protect RPE cells from CSE-induced ferroptosis, and this evidence paves the way for AMD studies.

* Corresponding author. The First Affiliated Hospital of Chongqing Medical University, Chongqing, 400016, China.
** Corresponding author. The First Affiliated Hospital of Chongqing Medical University, Chongqing, 400016, China.
E-mail addresses: duyong101001@163.com (Y. Du), pengh9@sina.com (H. Peng).
[1] Long Zhao and Ping Wu contributed equally to this work.

https://doi.org/10.1016/j.heliyon.2024.e38151
Received 10 May 2024; Received in revised form 31 August 2024; Accepted 18 September 2024
Available online 24 September 2024

1. Introduction

Age-related macular degeneration (AMD) is a degenerative neuropathy that is the leading cause of low vision and even blindness in the elderly population [1], and the number of AMD cases is expected to reach 288 million cases worldwide by 2040 [2,3]. As China's population ages, the number of AMD patients will continue to increase [4]. AMD includes geographic atrophy (GA) and neovascular AMD, with the latter accounting for 10 %–20 % of AMD cases, which can be treated with anti-vascular endothelial growth factor [5] (VEGF) drugs (e.g., ranibizumab, conbercept). There is currently no effective treatment for dry AMD [6] (dAMD), except for the recommended supplementation of antioxidant vitamins, zinc (zinc oxide or zinc sulfate), lutein, etc. [7]. Therefore, it is imperative to find new targets to improve the prognosis of patients with dAMD.

Cigarette smoking is a significant risk factor for AM and may have a dose-response relationship with AMD [8,9]. Cigarette smoke extract (CSE) can enter the circulatory system of smokers and has been widely used in studies in cellular and animal disease models [10]. In ocular diseases, CSE induces oxidative stress and lipid metabolism disorders by promoting the production of reactive oxygen species (ROS), the release of inflammatory cytokines and the deposition of autofluorescent substances, which induce RPE dysfunction and ultimately increase the chance of AMD [11–13]. However, the potential molecular mechanisms of CSE-induced cytotoxicity need to be elucidated.

Ferroptosis is a novel iron-dependent programmed cell death (PCD) modality distinct from apoptosis, necrosis, and autophagy, and was first proposed by Dixon et al., in 2012 [14]. Excess intracellular ferrous ions (Fe^{2+}) increase the production of iron-related ROS via the Fenton reaction, leading to lipid peroxidation (LP), which causes lethal cellular damage and eventually ferroptosis [15,16]. Under transmission electron microscopy (TEM), ferroptotic cells exhibit mitochondrial shrinkage, an increase in mitochondrial membrane density, and a decrease in the number of mitochondrial cristae [14]. Ferrostatin-1 (Fer-1) and liproxstatin-1 (Lip-1) are specific ferroptosis inhibitors [17] that can scavenge ROS and inhibit lipid peroxidation, reducing unstable iron in cells and restoring Gpx4 levels to regulate ferroptosis. In addition, ferroptosis can also be activated by some agonists [18] (e.g., sorafenib and erastin).

In recent years, there has been increasing evidence that ferroptosis is a potential pathogenic mechanism of many human diseases, including neurodegenerative diseases, cardiovascular system diseases, and tumors [19–21]. For example, tert-butyl hydroperoxide [22] (tBH) and sodium iodate [23] (SI) oxidants can induce ferroptosis in RPE cells. Exposure of lung epithelial cells and vascular smooth muscle cells (VSMCs) to CSE can also cause ferroptosis [24–26]. However, there is still no evidence on whether CSE-induced RPE cell damage is associated with ferroptosis. Therefore, it is crucial to explore the link between ferroptosis and RPE, which may be related to the pathogenesis of AMD.

2. Materials and methods

2.1. Cell culture

Human retinal pigment epithelial (ARPE-19) cells were obtained from the American Type Culture Collection (ATCC), using Dulbecco's modified Eagle's medium/F12 (DMEM/F12 1:1) containing 10 % fetal bovine serum (FBS) (Procell, Wuhan, China). The culture flasks were placed in a cell culture incubator (Thermo Fisher, USA) at 37 °C and 5 % CO2. ARPE-19 cells were pretreated with Fer-1 (10 μM) or Lip-1 (10 μM) for 2 h before CSE stimulation. The cells were stimulated with CSE for 24 h [23].

2.2. Reagents and antibodies

The lipid ROS scavengers Fer-1 and Lip-1 and the ferroptosis inducer erastin were purchased from MCE (Shanghai, China).

The primary antibodies were all rabbit polyclonal antibodies. Anti-transferrin receptor (TFR) (AF5343, 1:1000), anti-acyl-aoA synthetase long chain family member 4 (ACSL4) (DF12141, 1:1000), anti-solute carrier family 7 member 11 (SLC7A11/xCT) (DF12509, 1:1000), anti-glutathione peroxidase-4 (Gpx4) (DF6701, 1:1000), anti-ferritin heavy chain-1 (FTH1) (DF6278, 1:1000), anti-ferritin light chain (FTL) (DF6604, 1:1000), anti-β-actin antibody (AF7018, 1:1000), and goat anti-rabbit IgG H&L (S0001, 1:10000) were purchased from Affinity (Jiangsu, China). Anti-interleukin-1β (IL-1β) (WL00891, 1:1000), anti-cyclooxygenase-Cox2 (Cox2) (WL01750, 1:1000), anti-interleukin-6 (IL-6) (WL02841, 1:1000), anti-interleukin-8 (IL-8) (WL03074, 1:1000), anti-tumor necrosis factor-α (TNF-α) (WL01581, 1:1000), and anti-monocyte chemoattractant protein-1 (MCP-1) (WL02966, 1:1000) were purchased from Wanleibio (Shenyang, China).

2.3. Preparation of cigarette smoke extract (CSE)

We prepared CSE using Longfeng Chengxiang cigarettes (carbon monoxide, 14 mg; nicotine, 1.2 mg; tar, 13 mg; Chongqing, China) as previously described [27–31]. Briefly, the steps are as follows: the smoke from the combustion of one cigarette was dissolved into 1 ml of DMEM/F12 using a modified 50-ml syringe as an actuating device. The mixture was filtered using a 0.22-μm microporous filter (BIOFIL, Guangzhou, China) to remove large particulate impurities and bacteria, and the pH of the mixture was adjusted to approximately 7.4. The final CSE solution was labelled 100 % and stored at −80 °C.

2.4. Animals and treatments

Eight-week-old C57BL/6 male mice (20–25 g each) were purchased from Chongqing Medical University Laboratory Animal

Research Center (Chongqing, China). All mice were kept in a pathogen-free room. The mice were anesthetized by intraperitoneal injection of 1.5 % sodium pentobarbital (5 μl/g), and CSE (2 μl) was injected into the vitreous cavity under a microscope using a microinjection pump (Bolige, Shanghai, China). DMEM/F12 was injected as the control [11]. All experimental procedures were approved by the Ethics Committee of Chongqing Medical University (IACUC-CQMU-2023-0355). All experimental procedures were conducted in conformity with the institutional guidelines issued by the IACUC of NUCM and the ARRIVE guidelines.

2.5. Cell viability assay

Cell Counting Kit-8 (CCK-8, MCE Shanghai, China) is a WST-8-based reagent for assessing cell proliferation and toxicity. ARPE-19 cells (100 μl/well) were seeded in a 96-well plate and placed in a 37 °C incubator for 24 h. The medium was changed to serum-free medium containing CSE or other drugs, followed by incubation for 24 h. The cells were incubated in the dark in DMEM/F12 (100 μl/well) containing 10 % CCK-8 for 1–4 h. Absorbance values at 450 nm were acquired using a microplate reader (Thermo Fisher, USA). The formula for calculating cell viability was as follows: cell viability = (Asample - Ablank)/(Acontrol - Ablank) × 100 %.

2.6. Measurement of intracellular ROS levels

A ROS assay kit (Beyotime, Shanghai, China) was used to analyze intracellular ROS levels using the fluorescent probe DCFH-DA. Briefly, ARPE-19 cells were washed 3 times with PBS, and an appropriate amount of DCFH-DA solution was added (DCFH-DA was diluted with serum-free culture medium so that the final concentration was 10 μmol/L). The cells were placed in a 37 °C incubator for 30 min and then observed and photographed using a fluorescence microscope (Leica Microscope, Germany) or flow cytometry (Thermo Fisher, USA), during all procedures, the samples were protected from light.

2.7. Measurement of lipid peroxide (MDA) levels

A malondialdehyde kit (MDA, Beyotime, Shanghai, China) was used to analyze lipid peroxidation levels using TBA. ARPE-19 cells were lysed with RIPA lysis buffer (Servicebio, Wuhan, China) containing protease inhibitor (PMSF) for 30 min, and centrifuged at 12,000×*g* for 10 min at 4 °C. The supernatant was then mixed with the reagents, and the samples were added to a 96-well plate, after which absorbance values were measured at 532 nm using a microplate reader; the obtain values were used to calculate the MDA content in the samples.

2.8. Measurement of intracellular glutathione (GSH) levels

Glutathione (GSH, Solarbio, Beijing, China) was analyzed by collecting cells ($\geq 10^6$), repeatedly freeze-thawing 2–3 times (freezing in liquid nitrogen and lysing in 37 °C water), and centrifuging at 8000×*g* for 10 min at 4 °C. The supernatant was retained and placed on ice, and the protein concentration of the supernatant was determined. An appropriate amount of supernatant was mixed with reagents at the recommended ratios, and the samples were left to stand for 2 min at room temperature. The absorbance value was measured by a microplate reader, and then, the GSH content was calculated.

2.9. Assessment of intracellular Fe^{2+} levels

FerroOrange (Dojindo, Kumamoto, Japan) is a novel fluorescent probe for divalent ferrous ions (Fe^{2+}). ARPE-19 cells were washed 3 times with PBS. FerroOrange working solution at a concentration of 1 μmol/L was added to cells, and the cells were placed in an incubator for 30 min, and then observed under a fluorescence microscope.

2.10. Measurement of mitochondrial membrane potential (MMP) (JC-1)

JC-1 (Beyotime, Shanghai, China) is an ideal fluorescent probe for analyzing MMP (ΔΨm). ARPE-19 cells were seeded in a 6-well plate, JC-1 (1 ml) staining solution was added, and the cells were incubated for 20 min protected from light. The cells were then observed and photographed under a fluorescence microscope.

2.11. Western blotting (Wb) analysis

Wb is a method of detecting the expression of proteins in a sample based on the specific antigen-antibody binding. Briefly, proteins were extracted from ARPE-19 cells and mouse RPE-choroid-scleral complexes with RIPA lysis buffer containing protease inhibitors. Proteins were separated by 10%–15 % SDS-PAGE (cell: 20 μg; eyeball tissue: 40 μg), and the transferred to a 0.45-μm PVDF membrane (Millipore USA). The membrane wass blocked with 5 % skim milk for 2 h at room temperature and then incubated with primary antibodies (anti-TFR, anti-ACSL4, anti-Cox-2, anti-xCT, anti-Gpx4, anti-FTH1, anti-FTL, anti-β-actin, anti-IL-1β, anti-IL-6, anti-IL-8, anti-TNF-α, anti-MCP-1) at 4 °C overnight. The membrane was then incubated with a 1:10,000 dilution of secondary antibody for 1–2 h at room temperature. Protein bands were visualized using an ECL luminescence reagent (MCE Shanghai, China) and imaged with a gel imager (Thermo Fisher USA).

2.12. Immunofluorescence (IF)

IF is an experimental technique used for localizing antigenic substances in tissues or cells. ARPE-19 cells were fixed with 4 % paraformaldehyde for 15 min, permeabilized with Triton X-100 (0.5 %) for 5 min, blocked with 10 % goat serum for 1 h at room temperature, and then incubated with the target primary antibody overnight in a 4 °C freezer. The following day, the cells were incubated with a fluorescent secondary antibody (1:100 dilution) for 1 h at room temperature in the dark and then stained with DAPI

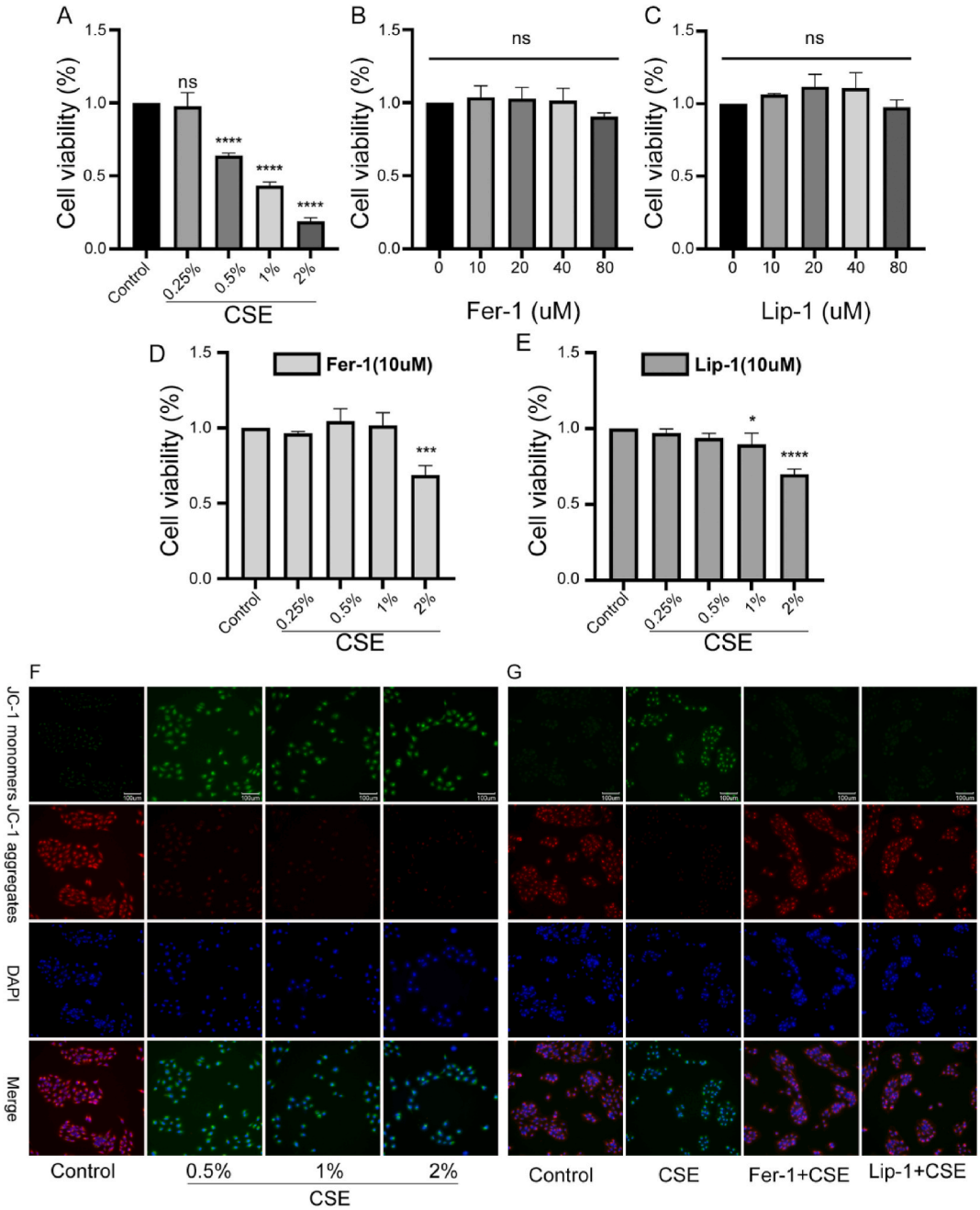

Fig. 1. CSE induces ARPE-19 cell death. A. ARPE-19 cells were stimulated with different concentrations of CSE for 24 h, and cell viability was determined using CCK-8 (n = 5). B and C. Cells were treated with ferroptosis inhibitors (Fer-1 and Lip-1) for 24 h with no significant cell death (n = 5). D and E. ARPE-19 cells were pretreated with ferroptosis inhibitors for 4 h and then cocultured with CSE for 24 h, and cell viability was determined (n = 5). F. Membrane potential changes were analyzed (JC-1 staining)in ARPE-19 cells after stimulation with different concentrations of CSE for 24 h. Green fluorescence indicates a decrease in MMP. G. Pretreatment of cells with Fer-1 and Lip-1 inhibited the decrease in the MMP. Scale bar: 100 μm.

for 5 min. Finally, an anti-fluorescence quencher was added dropwise, and the cells were observed and photographed using a fluorescence microscope.

2.13. Histological analysis

Mouse eyeballs were fixed in 4 % paraformaldehyde for 24 h, gradient dehydrated with ethanol, then embedded in paraffin and sliced into thin sections (5–8 μm thick) onto slides. Paraffin sections were deparaffinized, stained with hematoxylin-eosin (H&E) (Solarbio, Beijing, China) and lipofuscin, and fixed with resin. Finally, the tissue structure was observed and photographed under a microscope.

2.14. Transmission electron microscopy (TEM)

Cell microspheres (or mouse eyeballs) were placed in 2.5 % glutaraldehyde and fixed at 4 °C for 24 h. Then, they were set in 2 % osmium tetroxide (OsO4) for 1 h at room temperature, embedded in epoxy resin after gradient dehydration, cut into ultrathin sections (70–80 nm), soaked with uranyl acetate (1 %) and lead citrate (0.1 %), and observed and photographed by TEM (H-7700, Hitachi High-Technologies, Tokyo, Japan). Finally, the area, cristae number and circularity index of mitochondria were analyzed using Image J software.

2.15. Optical coherence tomography (OCT)

OCT can be used to generate fundus retina images and visualize RPE structures in the fundus. After anesthetizing the mice, the pupils were dilated with tropicamide, and then, the fundus was scanned using SS-OCT (VG200, Saiwei, China) to obtain fundus OCT images.

2.16. Electrophysiological detection (ERG)

C57BL/6 mice were placed in a dark room for more than 12 h, anesthetized, pupils dilated and other preparations were made, ERG (Yuyan Instrument, Shanghai, China) electrode pads were connected, and after the baseline was stabilized, the assay was carried out using different light stimulation intensities, and all the recorded wave forms and values were saved for analysis.

2.17. Statistical analysis

All experiments were replicated at least three times, and data were expressed as the mean ± standard deviation (SEM ± SD), with one-way analysis of variance (ANOVA) used for data with a normal distribution and two-way analysis of variance (ANOVA) used for comparisons among groups. Comparisons between groups were performed using unpaired t tests or ordinary two-way ANOVA. All statistical analyses were performed using GraphPad Prism 9.0 software (GraphPad, San Diego, CA, USA). $P < 0.05$ was considered statistically significant (*$P < 0.05$, **$P < 0.01$, ***$P < 0.001$, ****$P < 0.0001$, ns, no difference).

3. Results and figures

3.1. Ferroptosis inhibitors rescue CSE-induced RPE cell damage

To find suitable cell modeling conditions, we referred to previous studies and treated ARPE-19 cells with different concentrations of CSE (0, 0.25 %, 0.5 %, 1 %, 2 %) for 24 h and then assessed cell viability with CCK-8 [11]. We found that the viability of RPE cells decreased with increasing CSE concentration (Fig. 1 A). Based on the experimental results, we selected 0.5 % CSE as the modeling condition. Similarly, we found that certain concentrations of Fer-1 and Lip-1 did not significantly affect cell survival (Fig. 1B and C); 10 μM was selected as the most appropriate drug concentration. In addition, cell viability was better in the Fer-1+CSE and Lip-1+CSE groups than in the CSE group (Fig. 1D and E). The results suggested that ferroptosis inhibitors effectively protected against CSE-induced RPE cell damage.

To observe the contion of cellular mitochondria, we used JC-1 for fluorescence staining [32]. RPE cells in the CSE-exposed group mainly fluoreced green (Fig. 1 F and Fig.S1 D), indicating that the mitochondrial membrane structure was disrupted and dysfunctional, which caused a significant decrease in mitochondrial membrane potential (MMP). Nevertheless, the reduction in MMP was inhibited by Fer-1 and Lip-1 (Fig. 1 G and Fig.S1 E). We observed the ultrastructure of mitochondria using TEM, and the results showed that the ultrastructure of cells after CSE exposure was consistent with that of erastin-induced RPE cells. There was an overall shrinkage of cellular mitochondria, an increase in membrane density, and a decrease in number or loss of mitochondrial cristae [33] (Fig. 2 A and Fig.S1 A). In comparison, the pretreatment of RPE cells with Fer-1 and Lip-1 ameliorated mitochondrial membrane damage (Fig. 2 B).

3.2. CSE induces intracellular Fe^{2+} overload

Fe^{2+} overload is an essential feature of ferroptosis. We examined the intracellular Fe^{2+} level in RPE cells exposed to CSE using the FerroOrange fluorescent probe, and the results showed that intracellular fluorescence significantly increased after CSE exposure,

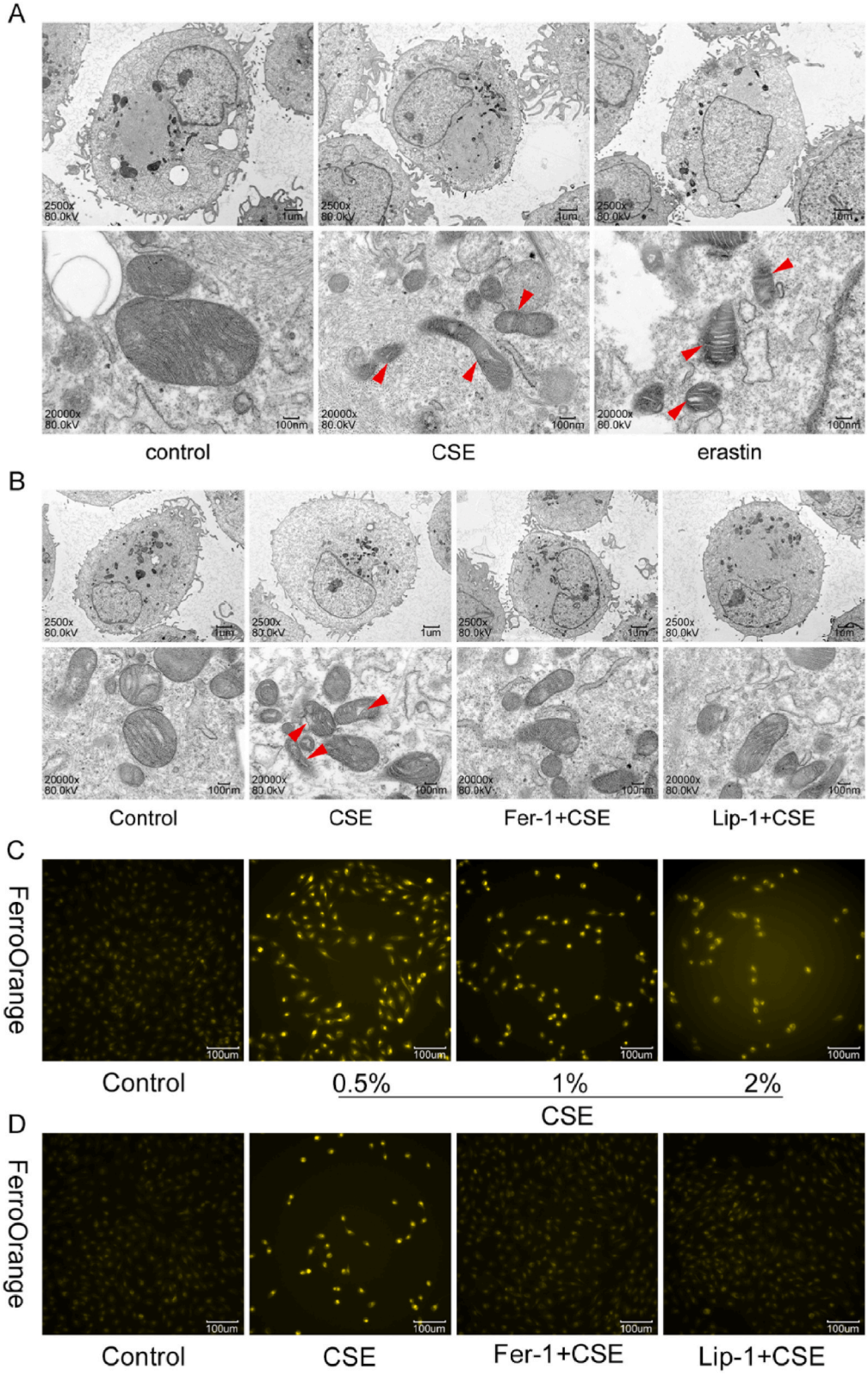

(caption on next page)

Fig. 2. CSE stimulates mitochondrial ultrastructural and intracellular Fe^{2+} changes in ARPE-19 cells. A. Cells were stimulated with 0.5 % CSE and 10 μM erastin for 24 h, and mitochondrial membrane structural alterations were observed by transmission electron microscopy (TEM) (shown by red arrows). B. Protective effects of Fer-1 and Lip-1 against CSE-induced mitochondrial injury. Scale: upper, 1 μm, lower, 100 μm. C. Cells were stimulated with CSE for 24 h, and FerroOrange was used to detect intracellular Fe^{2+}; yellow fluorescence indicates Fe^{2+} aggregation. D. Coculture with a ferroptosis inhibitor alleviated Fe^{2+} aggregation caused by CSE. Scale bar: 100 μm.

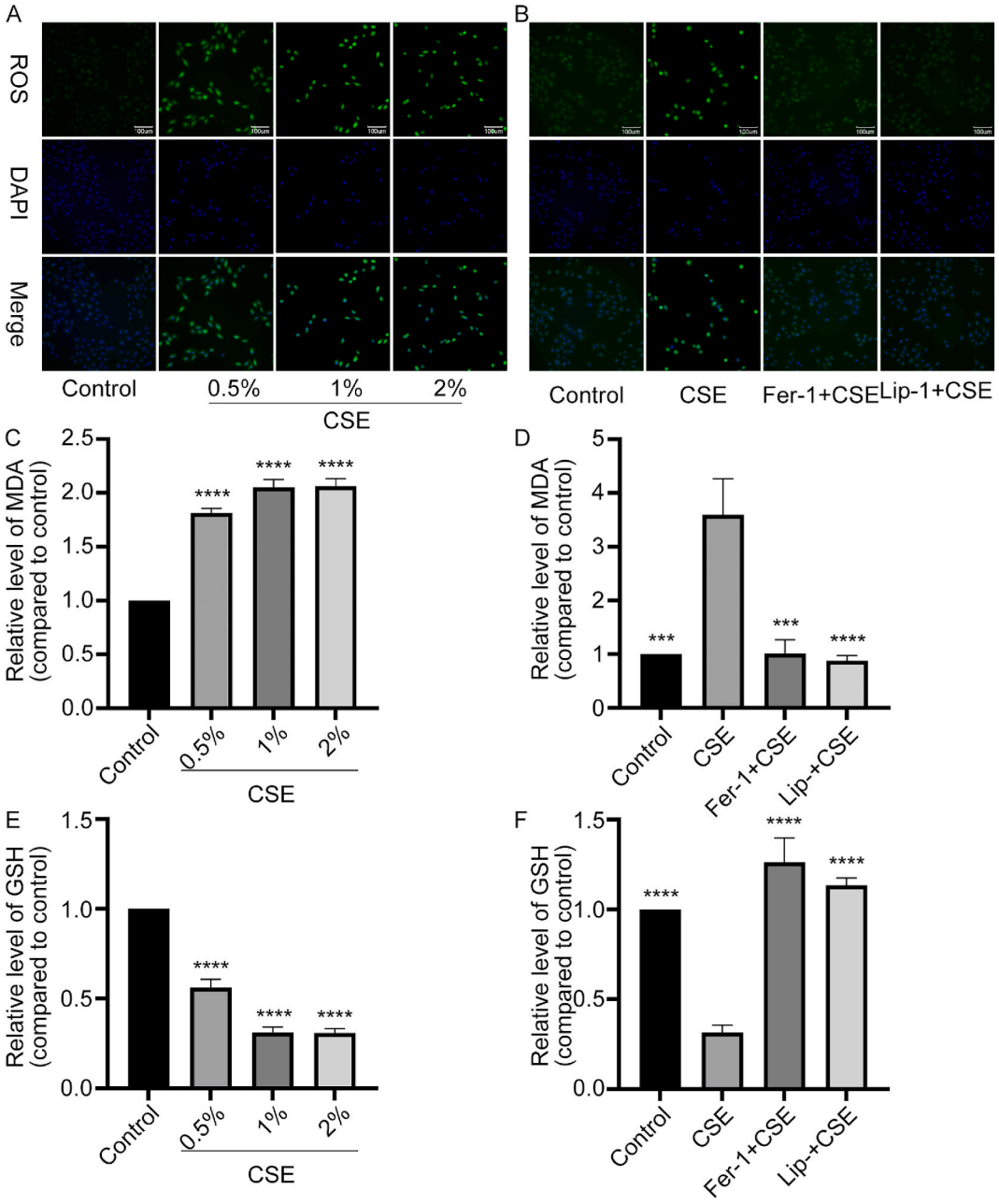

Fig. 3. CSE induces lipid peroxidation and GSH depletion in ARPE-19 cells. A. Cells with stimulated with CSE for 24 h and stained with the DCFH-DA probe (green fluorescent) for 30 min; fluorescence intensity was used to analyze ROS. Scale bar: 100 μm. C. Cells were treated with CSE for 24 h, and MDA levels were assesse using TBA. MDA levels are expressed as nmol/mg protein (n = 3). E. Cells were stimulated with CSE for 24 h, and GSH content was assessed using a GSH kit; GSH levels are expressed in μg/mg protein (n = 3). B, D, F. Pretreatment with a ferroptosis inhibitor reduced ROS aggregation, increased MDA levels, and decreased GSH levels.

suggesting that the Fe^{2+} level increased (Fig. 2 C). The level of Fe^{2+} decreased through the protective effects of Fer-1 and Lip-1 (Fig. 2 D).

3.3. CSE induces LP and GSH depletion

Ferroptosis is caused by the Fenton reaction, which induces ROS accumulation and lipid LP, with simultaneous GSH depletion. Therefore, we used the DCFH-DA probe to analyze intracellular ROS levels, and the results showed that green fluorescence (ROS) was significantly increased in the CSE group. Nevertheless, this increase was inhibited by Fer-1 and Lip-1 (Fig. 3A and B, Fig. S2). MDA is a hallmark product of LP, and it was found that the MDA level was significantly higher in cells exposed to CSE than in cells in the normal control group; this effect was concentration dependent (Fig. 3 C). The increase in MDA content was significantly inhibited by Fer-1 and Lip-1 (Fig. 3 D). GSH, a potent antioxidant, was significantly decreased in ARPE-19 cells after stimulation with CSE (Fig. 3 E); this effect was not observed after pretreatment with Fer-1 or Lip-1 (Fig. 3 F). Ferroptosis inhibitors alleviated ROS accumulation and LP, as well as GSH depletion, caused by CSE exposure.

3.4. Effects of CSE on the expression of ferroptosis- and inflammation-related proteins

We utilized Wb and IF to assess the expression of proteins related to ferroptosis and inflammation in CSE-treated ARPE-19 cells. The expression levels of ACSL4, an important isoenzyme of polyunsaturated fatty acid (PUFA) metabolism that determines the sensitivity of cells to ferroptosis, TFR, a transferrin receptor that mediates the transport of ferritin into cells, and Cox2, which is associated with oxidative stress and increases the production of ROS, leading to the intracellular release and accumulation of Fe^{2+}, were significantly increased in the CSE group. The protein levels of Xc^- system (xCT), which mediates cysteine entry into cells for GSH biosynthesis, Gpx4, which is an antioxidant defence protein, FTH1 and FTL, which play roles in the storage and regulation of Fe^{2+}, were decreased (Fig. 4 A and C). The expression of ferroptosis-related proteins was regulated by both Fer-1 and Lip-1 (Fig. 4B–D, and Fig. 5).

IL-1β, IL-6, IL-8, TNF-α, and MCP-1 are important inflammatory factors in the pathogenesis of AMD. The Wb results showed that

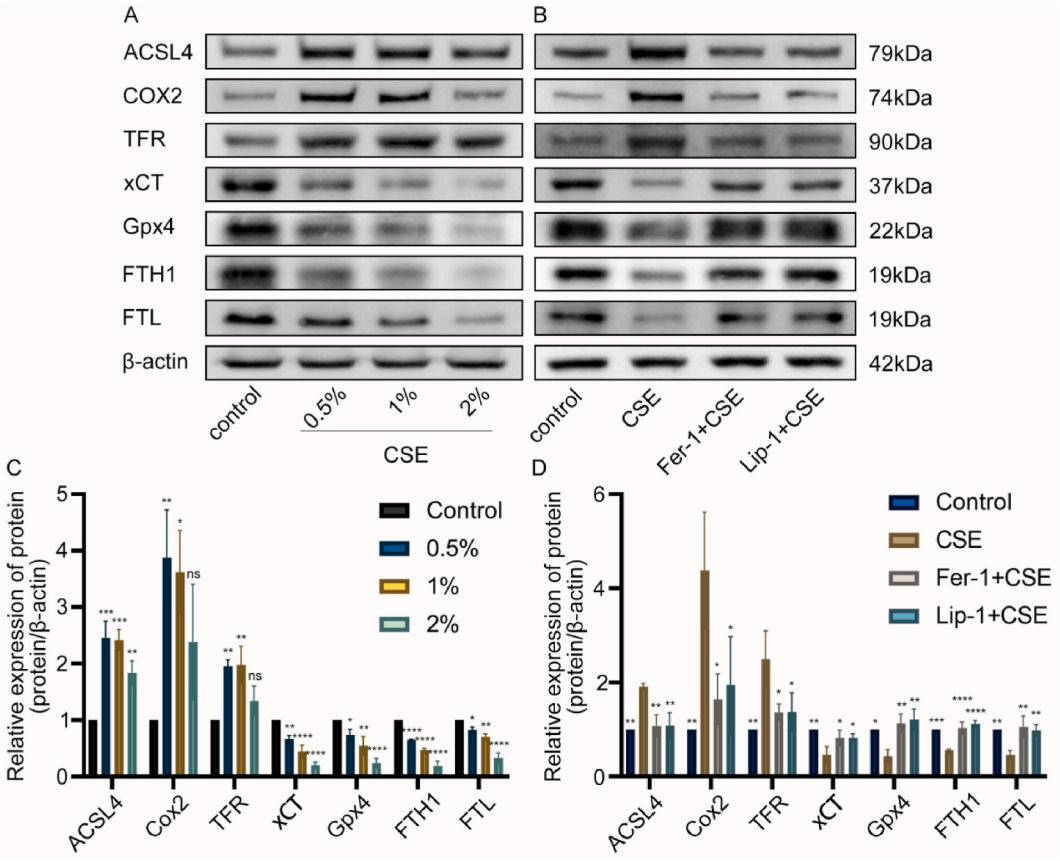

Fig. 4. Expression levels of ferroptosis-related proteins in ARPE-19 cells. A. Wb was used to assess the protein expression levels of ACSL4, Cox2, TFR, xCT, Gpx4, FTH1 and FTL in ARPE-19 cells after CSE (0.5 %) stimulation. C. Quantitative analysis of three replicate bands for A (n = 3, compared to the control group). B, D. The effect of ferroptosis inhibitors (10 μM) on the expression level of intracellular ferroptosis-related proteins caused by CSE and the quantitative analysis (n = 3, compared with the CSE group).

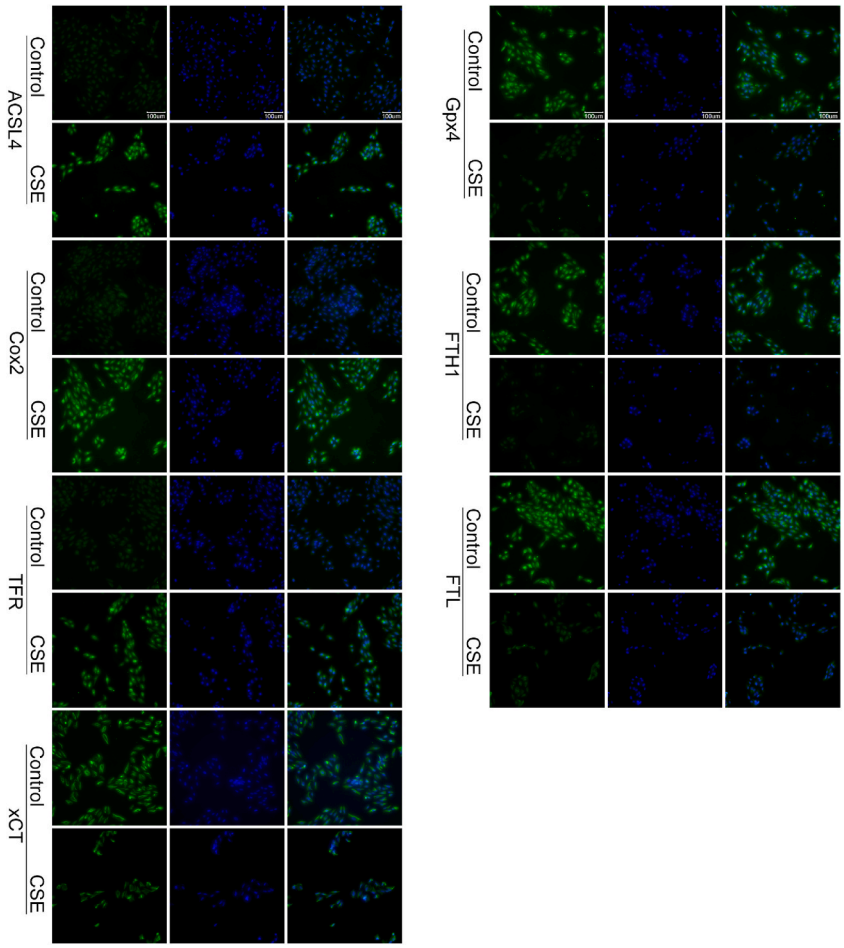

Fig. 5. Ferroptosis-related protein expression levels. The intracellular protein expression levels of ACSL4, Cox2, TFR, xCT, Gpx4, FTH1 and FTL proteins in ARPE-19 cells were analyzed by IF. Scale bar: 100 μm.

CSE exposure increased the expression level of inflammatory cytokines (Fig. 6 A and C). This finding It is consistent with the pathogenesis of AMD. Ferroptosis inhibitors ameliorate inflammation levels to some extent (Fig. 6 B and D). Ferroptosis inhibitors alleviated CSE-induced inflammation and ferroptosis in ARPE-19 cells.

3.5. CSE induces ferroptosis in vivo

To assess whether CSE induces the ferroptosis of RPE cells in vivo, we injected CSE into the vitreous cavity of C57BL/6 mice using a microsyringe, and removed the eyeballs after 7 days. H&E staining revealed the following: rupture of the RPE in the CSE group, impaired continuity of the RPE, and exudation and edema in the retina. Drusen appeared between the retina and RPE (Fig. 7 A). Lipofuscin staining revealed more lipofuscin granules in the CSE group than in the control mice (Fig. 7 C). We evaluated retinal function by electroretinogram to better correlate the effect of CSE with AMD, and discover that ERG a- and b-wave decreased in the CSE group (Fig.S1 B and C). Fundus OCT showed that the RPE and retina were damaged in mice in the CSE group (Fig. 7 B).

In addition, proteins from mouse RPE-choroid-scleral complex tissues were extracted for Wb experiments. We found that the expression levels of the ferroptosis-specific proteins ACSL4, Cox2 and TFR were increased but that the expression levels of xCT, Gpx4, FTH1 and FTL were decreased (Fig. 7D and E). Those findings are consistent with the results of the in vitro experiments. TEM also revealed apparent alterations in the mitochondria of RPE cells characterized by ferroptosis (Fig. 7 F). Similarly, ferroptosis inhibitors (Fer-1 and Lip-1) played a regulatory role in vivo.

4. Discussion

AMD is an irreversible degenerative disease that severely affects visual function and quality of life, and its pathogenesis is associated with oxidative stress and inflammation [34]. In addition to age, Fe^{2+} overload and CSE exposure are important environmental factors in the pathogenesis of AMD [35]. In previous studies, compared with non-AMD patients, patients with AMD had lipid

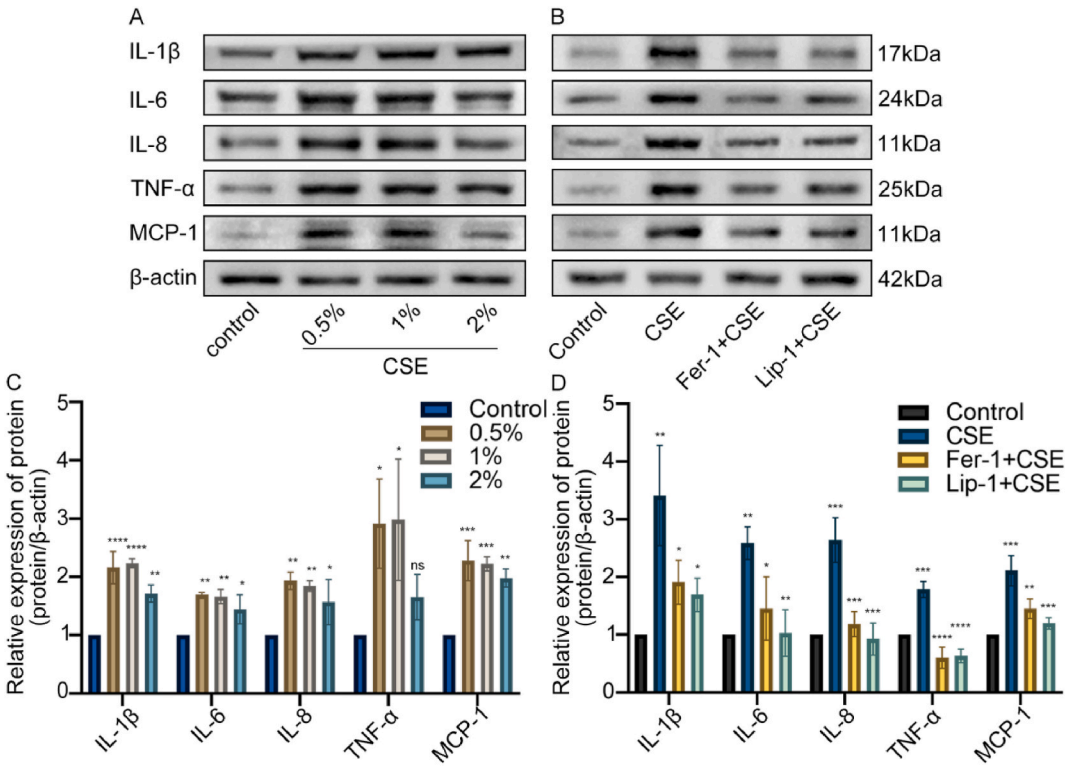

Fig. 6. Expression levels of inflammatory factor-related proteins. A. Wb assay was used to assess the protein expression levels of IL-1β, IL-6, IL-8, TNF-α and MCP-1 in ARPE-19 cells after CSE (0.5 %) stimulation. C. Quantitative analysis of three replicate bands for A (n = 3, compared to the control group). B, D. Ferroptosis inhibitors (10 μM) affect the expression level of intracellular inflammation-related proteins after exposure to CSE and the quantitative analysis (n = 3, compared with the CSE group).

deposition in the fundus [36], increased intracellular Fe^{2+} in RPE cells, and higher levels of Fe^{2+} and inflammatory factors in aqueous humor [37].

In this study, we found that CSE affects intracellular iron homeostasis, resulting in the accumulation of Fe^{2+}. The increase in ROS leads to lipid peroxidation and damage to the mitochondrial membrane structure and loss of mitochondrial membrane potential. Inhibition of the Xc^- transport system blocked the synthesis of GSH, and the antioxidant function of Gpx4 was inhibited. The activation of inflammatory cytokines results in damage to the RPE. In vivo experiments showed deterioration of the RPE and retinal structure, lipid metabolite deposition and mitochondrial injury, and altered expression of ferroptosis-related proteins. Fer-1 and Lip-1 ameliorated RPE injury caused by CSE.

CSE can affect RPE cell function through choroidal blood flow [26,38]. RPE cell dysfunction is the predominant pathogenic factor for AMD [39]. Therefore, we utilized an ARPE-19 cell model in this study to investigate the mechanism by which CSE induces RPE damage.

The concentration of CSE used in our study was 0.5 % (tar, 0.065 mg/mL; nicotine, 60 ng/ml), which has been shown to affect the survival of ARPE-19 cells [40]. In heavy smokers, the average blood nicotine concentration is 22 ng/mL. This indicates that the nicotine levels used in this study were relatively higher than the levels observed in actual human exposure [41]. In addition, the iron content in cigarette smoke is too low to cause iron to accumulate in the lungs or enter the bloodstream [42], thus excluding the accumulation of Fe^{2+} caused by CSE itself.

Ocular siderosis can damage the cornea, lens, and retina or cause irreversible vision loss [43]. Fe^{2+} has been shown to exacerbate the progression of retinal degeneration, and prolonged exposure to light increases the levels of Fe^{2+} in photoreceptor-derived cells in mice [44–46]. Intravitreal injections of Fe^{2+} in mice have been shown to induce photoreceptor death characteristic of ferroptosis, including increased lipid peroxidation and Cox2 (Ptgs2 mRNA) expression [47]. Iron chelating drugs can increase cone survival in mouse retinitis pigmentosa (RP) models [48]; they also attenuate neuronal loss and inhibit oxidative stress in animal models of Alzheimer's and Parkinson's diseases [49]. These insights suggest that Fe^{2+} levels may play important roles.

Through FerroOrange staining, we found compared with the control treatment, CSE caused a significant increase in the intracellular Fe^{2+} concentration in ARPE-19 cells; notably, this effect was affected by the CSE concentration. To understand how CSE affects the regulators of intracellular Fe^{2+}, we assessed the ferritin transport receptor (TFR) and storage proteins (FTH1 and FTL); the expression of the former was increased, increasing ferritin transport into the cell, and the expression of the latter was decreased, resulting in less ferritin binding and higher intracellular Fe^{2+} levels. In contrast, ferroptosis inhibitors blocked increases in Fe^{2+} levels

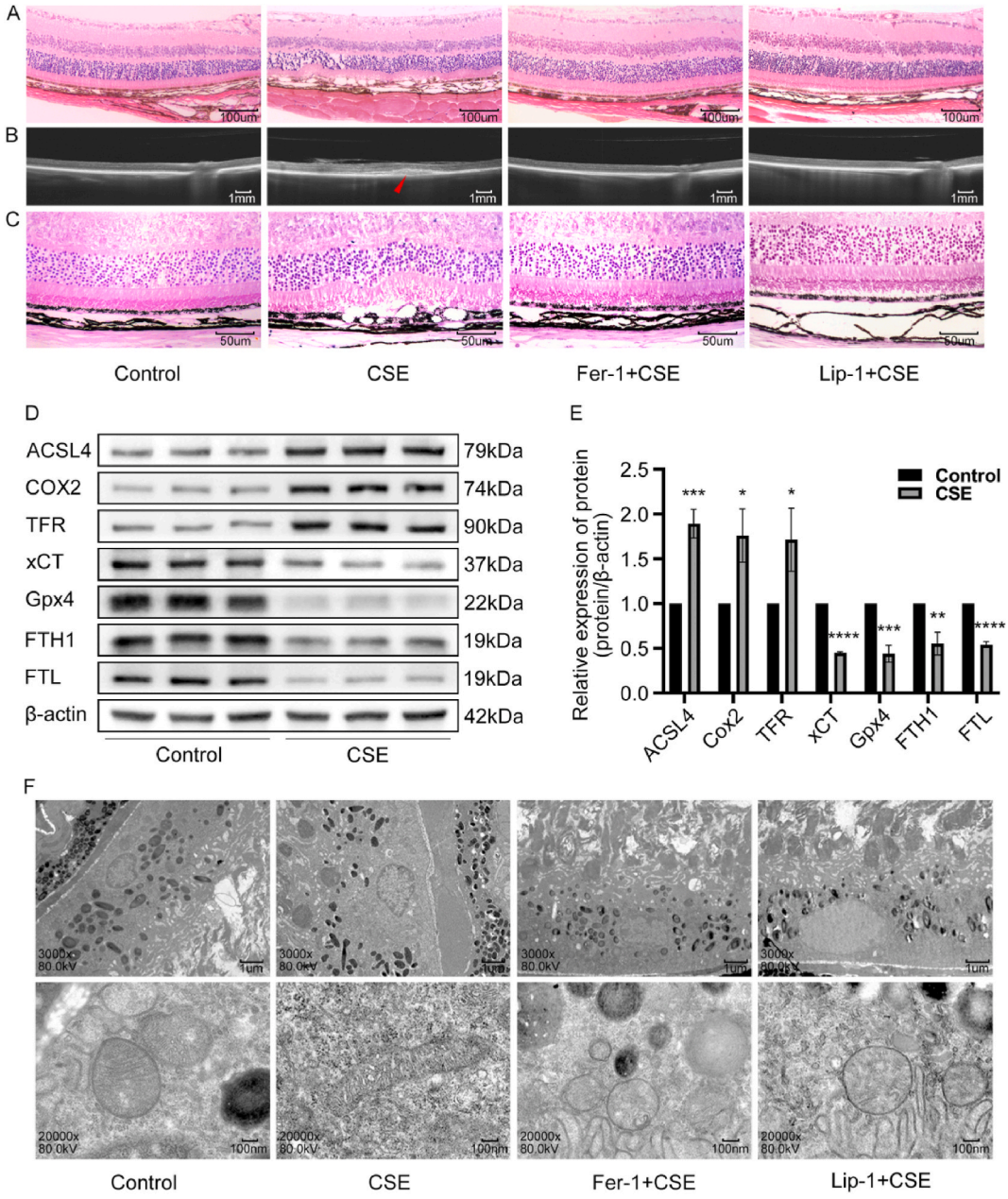

Fig. 7. CSE induces ferroptosis in vivo. A. C57BL/6 mice (n = 5) were injected with CSE intraocularly after being injected with a ferroptosis inhibitor 24 h prior. After modeling was completed, the eyeballs were removed for H&E staining after the modelling was completed to observe the structure of the retina and RPE. Scale bar: 100 μm. B. Mice were anesthetized, a fundus OCT scan was performed after pupil dilation, and fundus changes in living mice were observed (red arrow). Scale bar: 1 mm. C. Lipofuscin staining of paraffin sections of mouse eyeballs to identify retinal and RPE lipid metabolic deposits. Scale bar: 50 μm. D, E. Wb analysis of the protein expression levels of the mouse RPE-choroid-sclera complex, which contains ACSL4, Cox2, TFR, xCT, Gpx4, FTH1, and FTL, and the quantitative analysis. F Transmission electron microscopy (TEM) to observe mitochondrial structural changes in mouse RPE cells. Scale: upper, 1 μm, lower, 100 μm.

in ARPE-19 cells.

The results of other studies are consistent with our findings, i.e., that upregulation of TFR promotes extracellular ferritin uptake, and the downregulation of FTH1 and FTL as storage proteins releases bound ferritin and increases Fe^{2+} levels [50,51]. In addition, NaIO3 can increase intracellular labile iron levels (more than 40-fold) by oxidizing intracellular chelated iron (Fe-S protein) in RPE cells [23]. Thus, intracellular Fe^{2+} levels are a necessary factor in ferroptosis.

CSE-induced oxidative stress and lipid deposition act synergistically in the pathogenesis of AMD [11,36]. The accumulation of autofluorescent substances in human induced pluripotent stem cell-derived RPE (hiPSC-RPE) cells exposed to CSE is strong evidence of

the former [35]. In our experiments, using fluorescent probes, we found that CSE contributed to the increase in intracellular ROS in RPE cells, which in turn promoted lipid oxidation metabolism.

Phospholipids of polyunsaturated fatty acids (PUFAs) are substrates for ferroptosis lipid peroxidation, and ACSL4 promotes phospholipid biosynthesis [16,52,53]. Therefore, ACSL4 could determine ferroptosis sensitivity by altering the composition of cellular lipids. In our study, we found that the protein expression of ACSL4 was significantly increased in the CSE group and that the MDA produced during lipid metabolism increased with the increase in CSE concentration. In previous studies, CSE also increased intracellular MDA in RPE cells [36]. It has also been shown that ACSL4 knockdown leads to a decrease in substrates for lipid peroxidation, thereby increasing resistance to ferroptosis [54]. Thus, ACSL4 serves as a specific biomarker of ferroptosis and an essential regulator of lipid metabolism for ferroptosis [55].

Lipid peroxidation damages the plasma membrane, which is composed of phospholipids [56]. We analyzed the MMP using a JC-1 kit, and the results showed that the mitochondrial membrane was damaged and the membrane potential was significantly reduced in the CSE group. Moreover, alterations in mitochondrial ultrastructure, i.e., mitochondrial shrinkage, increase in membrane density, and decrease in or loss of cristae, were observed by TEM. Those findings are consistent with the alterations that are characteristic of ferroptosis.

GSH plays important roles, such as antioxidant and immunity enhancement [57]. In studies on ferroptosis in the cornea, N-acetylcysteine (NAC), a precursor of GSH, significantly attenuated corneal cell damage induced by CSE exposure, and NAC has been used clinically for the treatment of dry eye disease [43,58]. In our study, the GSH level significantly decreased after CSE exposure. To explore the mechanism by which GSH levels decrease, we examined the expression level of xCT in ARPE-19 cells using Wb and IF. xCT is an important component of the cystine-glutamate reverse transporter system (Xc^-) associated with GSH synthesis [59–62]. The results showed that the expression of xCT was significantly inhibited by CSE.

GPX4 is one of the earliest recognized and most studied regulators of lipid peroxidation [63,64]. GPX4 catalyzes not only the reduction of lipid peroxidation substrates but also the reduction of hydroperoxides in lipoproteins, complex lipids, and phospholipids [62,65]. Therefore, the antioxidant function of Gpx4 is particularly beneficial in tissues rich in polyunsaturated fatty acids, such as photoreceptors and RPE cells. In our experimental results, Gpx4 expression was significantly inhibited, indicating that severe lipid peroxidation occurred in the ARPE-19. Previous studies of Gpx4 and ferroptosis have shown that GPx4 overexpression attenuates CSE-induced lung injury in mouse models [66]. On the other hand, GPx4 deficiency also delays the healing of corneal epithelial wounds,an observation that coincides with our results [67].

GSH serves as an essential cofactor for Gpx4 to catalyze hydrogen peroxide [25], and GSH depletion may lead to the inactivation of Gpx4. This shows that xCT-GSH-Gpx4 is not only a marker of ferroptosis but also an important regulator. This was also demonstrated in our study, and lipid peroxidation was inhibited in ARPE-19 cells under the protective effect of ferroptosis inhibitors.

The upregulation of Cox2 (Ptgs2 mRNA) is a downstream manifestation of lipid peroxidation during ferroptosis, and Ptgs2 has been identified as a key gene for ferroptosis in several studies [68,69]. Likewise, the upregulation of Cox2 expression in RPE cells was observed in our study, indirectly demonstrating that the cells underwent lipid peroxidation. In addition, inflammatory factors not only play an important roles in the pathogenesis of AMD, but are also closely associated with cellular ferroptosis [70,71]. In our study, CSE increased the expression of IL-1β, IL-6, IL-8, TNF-α, and MCP-1 in ARPE-19 cells; however, the inhibition of ferroptosis reduced the expression of inflammatory cytokines in RPE cells. It has also been reported that IL-8 levels are increased in bronchoalveolar lavage fluid from healthy smokers and chronic obstructive pulmonary disease (COPD) patients [42], as are the levels of IL-1 and tumor necrosis factor-α (TNF-α), which are correlated with IL-8 expression [72]. These results suggest that exposure to CSE induces abnormal inflammation, providing strong evidence for the CSE-induced elevation of inflammatory factors in RPE cells.

We established an in vivo mouse model by the intraocular injection of CSE (0.5 %/2 μl) in C57BL/6 mice. The ferroptosis inhibitor group was injected with inhibitor 24 h prior to the injection of CSE. We observed RPE disruption and retinal exudative edema on fundus OCT and H&E staining. Lipid metabolite deposition was observed by lipofuscin staining. Wb was used to assess the expression of RPE-choroid-scleral complex proteins, and the results showed that the expression of ferroptosis-related proteins was affected by CSE. The mitochondrial ultrastructural changes observed by TEM were consistent with those observed in in vitro experiments. Moreover, the inhibition of ferroptosis alleviated the RPE damage caused by CSE to a certain extent. The above results of the in vitro and in vivo experiments were characteristic of ferroptosis.

However, this study has certain limitations. The sample size was small and should be further expanded in future studies. The boundaries of the experimental environment should be delineated through clinical investigations. Experimental data error can be reduced by increasing the number of repeated experiments.

5. Conclusion

Our results suggest that CSE exposure affected the expression level of intracellular Fe^{2+} regulatory proteins in RPE cells, causing intracellular Fe^{2+} overload, resulting in an increase in iron-related ROS, lipid peroxidation, mitochondrial membrane damage and lipid metabolite deposition in the RPE cells. Furthermore, CSE inhibited the Xc^- transport system, reduced GSH synthesis and thus inhibited Gpx4 antioxidant enzyme activity. At the same time, it induced the expression of inflammatory factors, resulting in damage to RPE cells and the retina. In conclusion, this is the first study to demonstrate that CSE induces ferroptosis in RPE cells, and indicate that changes in RPE might be of relevance for AMD pathology.

Funding

Supported by grants from the National Natural Science Foundation of China (no. 81670881).

Data availability statement

The datasets analyzed during the present study are available from the corresponding author onreasonable request.

Ethical approval

The present study was approved by the Ethics Committee of The First Affiliated Hospital of Chongqing Medical University (Chongqing, China, IACUC-CQMU-2023-0355).

CRediT authorship contribution statement

Long Zhao: Writing – original draft, Methodology, Data curation. **Ping Wu:** Writing – original draft, Resources, Formal analysis. **Jing Lu:** Software. **Yuxia He:** Resources. **Qinxin Shu:** Investigation. **Fuying Pan:** Data curation. **Hao Xie:** Software. **Xing Wang:** Supervision. **Huan Ju:** Resources. **Yong Du:** Writing – review & editing, Project administration. **Hui Peng:** Writing – review & editing, Funding acquisition.

Declaration of competing interest

We declare that we have no known competing financial interests or personal relationships that could have appeared to influence the work reported in this paper.

Appendix A. Supplementary data

Supplementary data to this article can be found online at https://doi.org/10.1016/j.heliyon.2024.e38151.

References

[1] C.J. Flaxel, R.A. Adelman, S.T. Bailey, A. Fawzi, J.I. Lim, G.A. Vemulakonda, G.S. Ying, Age-related macular degeneration preferred practice Pattern®, Ophthalmology 127 (2020) P1–p65.
[2] W.L. Wong, X. Su, X. Li, C.M. Cheung, R. Klein, C.Y. Cheng, T.Y. Wong, Global prevalence of age-related macular degeneration and disease burden projection for 2020 and 2040: a systematic review and meta-analysis, Lancet Glob Health 2 (2014) e106–e116.
[3] H. Ye, Q. Zhang, X. Liu, X. Cai, W. Yu, S. Yu, T. Wang, W. Lu, X. Li, H. Jin, et al., Prevalence of age-related macular degeneration in an elderly urban Chinese population in China: the Jiangning Eye Study, Invest. Ophthalmol. Vis. Sci. 55 (2014) 6374–6380.
[4] T. Xu, B. Wang, H. Liu, H. Wang, P. Yin, W. Dong, J. Li, Y.X. Wang, M. Yusufu, P. Briant, et al., Prevalence and causes of vision loss in China from 1990 to 2019: findings from the global burden of disease study 2019, Lancet Public Health 5 (2020) e682–e691.
[5] C.J. Thomas, R.G. Mirza, M.K. Gill, Age-related macular degeneration, Med Clin North Am 105 (2021) 473–491.
[6] R. Flores, Â. Carneiro, M. Vieira, S. Tenreiro, M.C. Seabra, Age-related macular degeneration: pathophysiology, management, and future perspectives, Ophthalmologica 244 (2021) 495–511.
[7] Lutein + zeaxanthin and omega-3 fatty acids for age-related macular degeneration: the Age-Related Eye Disease Study 2 (AREDS2) randomized clinical trial, JAMA 309 (2013) 2005–2015.
[8] J.C. Khan, D.A. Thurlby, H. Shahid, D.G. Clayton, J.R. Yates, M. Bradley, A.T. Moore, A.C. Bird, Smoking and age related macular degeneration: the number of pack years of cigarette smoking is a major determinant of risk for both geographic atrophy and choroidal neovascularisation, Br. J. Ophthalmol. 90 (2006) 75–80.
[9] T.E. Clemons, R.C. Milton, R. Klein, J.M. Seddon, F.L. Ferris, 3rd: **risk factors for the incidence of advanced age-related macular degeneration in the age-related eye disease study (AREDS) AREDS report no. 19**, Ophthalmology 112 (2005) 533–539.
[10] C. Huang, J.J. Wang, J.H. Ma, C. Jin, Q. Yu, S.X. Zhang, Activation of the UPR protects against cigarette smoke-induced RPE apoptosis through up-regulation of Nrf2, J. Biol. Chem. 290 (2015) 5367–5380.
[11] S.H. Kim, J.W. Park, Morin hydrate attenuates CSE-induced lipid accumulation, ER stress, and oxidative stress in RPE cells: implications for age-related macular degeneration, Free Radic. Res. 53 (2019) 865–874.
[12] A.L. Yu, K. Birke, J. Burger, U. Welge-Lussen, Biological effects of cigarette smoke in cultured human retinal pigment epithelial cells, PLoS One 7 (2012) e48501.
[13] M.C. Marazita, A. Dugour, M.D. Marquioni-Ramella, J.M. Figueroa, A.M. Suburo, Oxidative stress-induced premature senescence dysregulates VEGF and CFH expression in retinal pigment epithelial cells: implications for Age-related Macular Degeneration, Redox Biol. 7 (2016) 78–87.
[14] S.J. Dixon, K.M. Lemberg, M.R. Lamprecht, R. Skouta, E.M. Zaitsev, C.E. Gleason, D.N. Patel, A.J. Bauer, A.M. Cantley, W.S. Yang, et al., Ferroptosis: an iron-dependent form of nonapoptotic cell death, Cell 149 (2012) 1060–1072.
[15] J. Liu, R. Kang, D. Tang, Signaling pathways and defense mechanisms of ferroptosis, FEBS J. 289 (2022) 7038–7050.
[16] B.R. Stockwell, J.P. Friedmann Angeli, H. Bayir, A.I. Bush, M. Conrad, S.J. Dixon, S. Fulda, S. Gascón, S.K. Hatzios, V.E. Kagan, et al., Ferroptosis: a regulated cell death nexus linking metabolism, redox biology, and disease, Cell 171 (2017) 273–285.
[17] Y. Luo, X. Gao, L. Zou, M. Lei, J. Feng, Z. Hu, Bavachin induces ferroptosis through the STAT3/P53/SLC7A11 Axis in osteosarcoma cells, Oxid. Med. Cell. Longev. 2021 (2021) 1783485.
[18] H. Lee, F. Zandkarimi, Y. Zhang, J.K. Meena, J. Kim, L. Zhuang, S. Tyagi, L. Ma, T.F. Westbrook, G.R. Steinberg, et al., Energy-stress-mediated AMPK activation inhibits ferroptosis, Nat. Cell Biol. 22 (2020) 225–234.
[19] X. Fang, H. Wang, D. Han, E. Xie, X. Yang, J. Wei, S. Gu, F. Gao, N. Zhu, X. Yin, et al., Ferroptosis as a target for protection against cardiomyopathy, Proc Natl Acad Sci U S A 116 (2019) 2672–2680.

[20] Y. Zhang, J. Shi, X. Liu, L. Feng, Z. Gong, P. Koppula, K. Sirohi, X. Li, Y. Wei, H. Lee, et al., BAP1 links metabolic regulation of ferroptosis to tumour suppression, Nat. Cell Biol. 20 (2018) 1181–1192.
[21] B. DoVan, F. Gouel, A. Jonneaux, K. Timmerman, P. Gelé, M. Pétrault, M. Bastide, C. Laloux, C. Moreau, R. Bordet, et al., Ferroptosis, a newly characterized form of cell death in Parkinson's disease that is regulated by PKC, Neurobiol. Dis. 94 (2016) 169–178.
[22] K. Totsuka, T. Ueta, T. Uchida, M.F. Roggia, S. Nakagawa, D.G. Vavvas, M. Honjo, M. Aihara, Oxidative stress induces ferroptotic cell death in retinal pigment epithelial cells, Exp. Eye Res. 181 (2019) 316–324.
[23] B. Liu, W. Wang, A. Shah, M. Yu, Y. Liu, L. He, J. Dang, L. Yang, M. Yan, Y. Ying, et al., Sodium iodate induces ferroptosis in human retinal pigment epithelium ARPE-19 cells, Cell Death Dis. 12 (2021) 230.
[24] X. Tang, Z. Li, Z. Yu, J. Li, J. Zhang, N. Wan, J. Zhang, J. Cao, Effect of curcumin on lung epithelial injury and ferroptosis induced by cigarette smoke, Hum. Exp. Toxicol. 40 (2021) S753–s762.
[25] N. Lian, Q. Zhang, J. Chen, M. Chen, J. Huang, Q. Lin, The role of ferroptosis in bronchoalveolar epithelial cell injury induced by cigarette smoke extract, Front. Physiol. 12 (2021) 751206.
[26] A. Sampilvanjil, T. Karasawa, N. Yamada, T. Komada, T. Higashi, C. Baatarjav, S. Watanabe, R. Kamata, N. Ohno, M. Takahashi, Cigarette smoke extract induces ferroptosis in vascular smooth muscle cells, Am. J. Physiol. Heart Circ. Physiol. 318 (2020) H508–h518.
[27] X. Liu, Y. Ma, L. Luo, D. Zong, H. Li, Z. Zeng, Y. Cui, W. Meng, Y. Chen, Dihydroquercetin suppresses cigarette smoke induced ferroptosis in the pathogenesis of chronic obstructive pulmonary disease by activating Nrf2-mediated pathway, Phytomedicine 96 (2022) 153894.
[28] T. Di, Y. Yang, C. Fu, Z. Zhang, C. Qin, X. Sai, J. Liu, C. Hu, M. Zheng, Y. Wu, T. Bian, Let-7 mediated airway remodelling in chronic obstructive pulmonary disease via the regulation of IL-6, Eur. J. Clin. Invest. 51 (2021) e13425.
[29] P. Pavlou, I. Antoniadou, A. Peraki, A. Vitsos, P. Dallas, D. Mostratos, G. Deliconstantinos, G. Papaioannou, S.A. Grando, M. Rallis, Protective effects of pinus halepensis bark extract and nicotine on cigarette smoke-induced oxidative stress in keratinocytes, in: In Vivo, vol. 34, 2020, pp. 1835–1843.
[30] Y. Ma, L. Luo, X. Liu, H. Li, Z. Zeng, X. He, Z. Zhan, Y. Chen, Pirfenidone mediates cigarette smoke extract induced inflammation and oxidative stress in vitro and in vivo, Int Immunopharmacol 96 (2021) 107593.
[31] L. Chen, L. Luo, N. Kang, X. He, T. Li, Y. Chen, The protective effect of HBO1 on cigarette smoke extract-induced apoptosis in airway epithelial cells, Int J Chron Obstruct Pulmon Dis 15 (2020) 15–24.
[32] Y. Zi, X. Wang, Y. Zi, H. Yu, Y. Lan, Y. Fan, C. Ren, K. Liao, H. Chen, Cigarette smoke induces the ROS accumulation and iNOS activation through deactivation of Nrf-2/SIRT3 axis to mediate the human bronchial epithelium ferroptosis, Free Radic. Biol. Med. 200 (2023) 73–86.
[33] J. Lam, P. Katti, M. Biete, M. Mungai, S. AshShareef, K. Neikirk, E. Garza Lopez, Z. Vue, T.A. Christensen, H.K. Beasley, et al., A universal approach to analyzing transmission electron microscopy with ImageJ, Cells 10 (2021).
[34] R.H. Guymer, T.G. Campbell, Age-related macular degeneration, Lancet 401 (2023) 1459–1472.
[35] S. Dalvi, C.A. Galloway, L. Winschel, A. Hashim, C. Soto, C. Tang, L.A. MacDonald, R. Singh, Environmental stress impairs photoreceptor outer segment (POS) phagocytosis and degradation and induces autofluorescent material accumulation in hiPSC-RPE cells, Cell Death Discov 5 (2019) 96.
[36] K. Kunchithapautham, C. Atkinson, B. Rohrer, Smoke exposure causes endoplasmic reticulum stress and lipid accumulation in retinal pigment epithelium through oxidative stress and complement activation, J. Biol. Chem. 289 (2014) 14534–14546.
[37] D. Song, J.L. Dunaief, Retinal iron homeostasis in health and disease, Front. Aging Neurosci. 5 (2013) 24.
[38] Y. Yamaguchi, F. Nasu, A. Harada, M. Kunitomo, Oxidants in the gas phase of cigarette smoke pass through the lung alveolar wall and raise systemic oxidative stress, J. Pharmacol. Sci. 103 (2007) 275–282.
[39] C. Huang, J.J. Wang, G. Jing, J. Li, C. Jin, Q. Yu, M.W. Falkowski, S.X. Zhang, Erp29 attenuates cigarette smoke extract-induced endoplasmic reticulum stress and mitigates tight junction damage in retinal pigment epithelial cells, Invest. Ophthalmol. Vis. Sci. 56 (2015) 6196–6207.
[40] K.M. Bertram, C.J. Baglole, R.P. Phipps, R.T. Libby, Molecular regulation of cigarette smoke induced-oxidative stress in human retinal pigment epithelial cells: implications for age-related macular degeneration, Am J Physiol Cell Physiol 297 (2009) C1200–C1210.
[41] N.L. Benowitz, F. Kuyt, P. Jacob 3rd, R.T. Jones, A.L. Osman, Cotinine disposition and effects, Clin. Pharmacol. Ther. 34 (1983) 604–611.
[42] A.J. Ghio, E.D. Hilborn, J.G. Stonehuerner, L.A. Dailey, J.D. Carter, J.H. Richards, K.M. Crissman, R.F. Foronjy, D.L. Uyeminami, K.E. Pinkerton, Particulate matter in cigarette smoke alters iron homeostasis to produce a biological effect, Am. J. Respir. Crit. Care Med. 178 (2008) 1130–1138.
[43] W. Otsu, K. Ishida, N. Chinen, S. Nakamura, M. Shimazawa, H. Tsusaki, H. Hara, Cigarette smoke extract and heated tobacco products promote ferritin cleavage and iron accumulation in human corneal epithelial cells, Sci. Rep. 11 (2021) 18555.
[44] T. Zhao, X. Guo, Y. Sun, Iron accumulation and lipid peroxidation in the aging retina: implication of ferroptosis in age-related macular degeneration, Aging Dis 12 (2021) 529–551.
[45] T. Imamura, T. Hirayama, K. Tsuruma, M. Shimazawa, H. Nagasawa, H. Hara, Hydroxyl radicals cause fluctuation in intracellular ferrous ion levels upon light exposure during photoreceptor cell death, Exp. Eye Res. 129 (2014) 24–30.
[46] X. He, P. Hahn, J. Iacovelli, R. Wong, C. King, R. Bhisitkul, M. Massaro-Giordano, J.L. Dunaief, Iron homeostasis and toxicity in retinal degeneration, Prog. Retin. Eye Res. 26 (2007) 649–673.
[47] W. Shu, B.H. Baumann, Y. Song, Y. Liu, X. Wu, J.L. Dunaief, Ferrous but not ferric iron sulfate kills photoreceptors and induces photoreceptor-dependent RPE autofluorescence, Redox Biol. 34 (2020) 101469.
[48] K. Wang, B. Peng, J. Xiao, O. Weinreb, M.B.H. Youdim, B. Lin, Iron-chelating drugs enhance cone photoreceptor survival in a mouse model of retinitis pigmentosa, Invest. Ophthalmol. Vis. Sci. 58 (2017) 5287–5297.
[49] O. Bar-Am, T. Amit, L. Kupershmidt, Y. Aluf, D. Mechlovich, H. Kabha, L. Danovitch, V.R. Zurawski, M.B. Youdim, O. Weinreb, Neuroprotective and neurorestorative activities of a novel iron chelator-brain selective monoamine oxidase-A/monoamine oxidase-B inhibitor in animal models of Parkinson's disease and aging, Neurobiol. Aging 36 (2015) 1529–1542.
[50] Y. Kang, R. Zhu, S. Li, K.P. Qin, H. Tang, W.S. Shan, Z.S. Yin, Erythropoietin inhibits ferroptosis and ameliorates neurological function after spinal cord injury, Neural Regen Res 18 (2023) 881–888.
[51] X. Chen, C. Gao, Y. Yan, Z. Cheng, G. Chen, T. Rui, C. Luo, Y. Gao, T. Wang, X. Chen, L. Tao, Ruxolitinib exerts neuroprotection via repressing ferroptosis in a mouse model of traumatic brain injury, Exp. Neurol. 342 (2021) 113762.
[52] Y. Yang, T. Zhu, X. Wang, F. Xiong, Z. Hu, X. Qiao, X. Yuan, D. Wang, ACSL3 and ACSL4, distinct roles in ferroptosis and cancers, Cancers 14 (2022).
[53] S. Doll, B. Proneth, Y.Y. Tyurina, E. Panzilius, S. Kobayashi, I. Ingold, M. Irmler, J. Beckers, M. Aichler, A. Walch, et al., ACSL4 dictates ferroptosis sensitivity by shaping cellular lipid composition, Nat. Chem. Biol. 13 (2017) 91–98.
[54] Y. Wang, M. Zhang, R. Bi, Y. Su, F. Quan, Y. Lin, C. Yue, X. Cui, Q. Zhao, S. Liu, et al., ACSL4 deficiency confers protection against ferroptosis-mediated acute kidney injury, Redox Biol. 51 (2022) 102262.
[55] H. Yuan, X. Li, X. Zhang, R. Kang, D. Tang, Identification of ACSL4 as a biomarker and contributor of ferroptosis, Biochem. Biophys. Res. Commun. 478 (2016) 1338–1343.
[56] L.J. Su, J.H. Zhang, H. Gomez, R. Murugan, X. Hong, D. Xu, F. Jiang, Z.Y. Peng, Reactive oxygen species-induced lipid peroxidation in apoptosis, autophagy, and ferroptosis, Oxid. Med. Cell. Longev. 2019 (2019) 5080843.
[57] Y. Sun, Y. Zheng, C. Wang, Y. Liu, Glutathione depletion induces ferroptosis, autophagy, and premature cell senescence in retinal pigment epithelial cells, Cell Death Dis. 9 (2018) 753.
[58] J. Haut, P. Labrune, M. Ullern, M. Chermet, New trial treatment of dry eye with acetylcysteine ophthalmic solution, Bull. Soc. Ophtalmol. Fr. 77 (1977) 165–167.
[59] P. Koppula, L. Zhuang, B. Gan, Cystine transporter SLC7A11/xCT in cancer: ferroptosis, nutrient dependency, and cancer therapy, Protein Cell 12 (2021) 599–620.
[60] S. Okazaki, K. Umene, J. Yamasaki, K. Suina, Y. Otsuki, M. Yoshikawa, Y. Minami, T. Masuko, S. Kawaguchi, H. Nakayama, et al., Glutaminolysis-related genes determine sensitivity to xCT-targeted therapy in head and neck squamous cell carcinoma, Cancer Sci. 110 (2019) 3453–3463.

[61] M. Gao, P. Monian, Q. Pan, W. Zhang, J. Xiang, X. Jiang, Ferroptosis is an autophagic cell death process, Cell Res. 26 (2016) 1021–1032.
[62] X. Jiang, B.R. Stockwell, M. Conrad, Ferroptosis: mechanisms, biology and role in disease, Nat. Rev. Mol. Cell Biol. 22 (2021) 266–282.
[63] Y. Zhang, B.Y. Fan, Y.L. Pang, W.Y. Shen, X. Wang, C.X. Zhao, W.X. Li, C. Liu, X.H. Kong, G.Z. Ning, et al., Neuroprotective effect of deferoxamine on erastininduced ferroptosis in primary cortical neurons, Neural Regen Res 15 (2020) 1539–1545.
[64] W.S. Hambright, R.S. Fonseca, L. Chen, R. Na, Q. Ran, Ablation of ferroptosis regulator glutathione peroxidase 4 in forebrain neurons promotes cognitive impairment and neurodegeneration, Redox Biol. 12 (2017) 8–17.
[65] W.S. Yang, R. SriRamaratnam, M.E. Welsch, K. Shimada, R. Skouta, V.S. Viswanathan, J.H. Cheah, P.A. Clemons, A.F. Shamji, C.B. Clish, et al., Regulation of ferroptotic cancer cell death by GPX4, Cell 156 (2014) 317–331.
[66] M. Yoshida, S. Minagawa, J. Araya, T. Sakamoto, H. Hara, K. Tsubouchi, Y. Hosaka, A. Ichikawa, N. Saito, T. Kadota, et al., Involvement of cigarette smoke-induced epithelial cell ferroptosis in COPD pathogenesis, Nat. Commun. 10 (2019) 3145.
[67] O. Sakai, T. Uchida, H. Imai, T. Ueta, Glutathione peroxidase 4 plays an important role in oxidative homeostasis and wound repair in corneal epithelial cells, FEBS Open Bio 6 (2016) 1238–1247.
[68] A. Sengupta, U.F. Lichti, B.A. Carlson, C. Cataisson, A.O. Ryscavage, C. Mikulec, M. Conrad, S.M. Fischer, D.L. Hatfield, S.H. Yuspa, Targeted disruption of glutathione peroxidase 4 in mouse skin epithelial cells impairs postnatal hair follicle morphogenesis that is partially rescued through inhibition of COX-2, J. Invest. Dermatol. 133 (2013) 1731–1741.
[69] T. Kumagai, N. Matsukawa, Y. Kaneko, Y. Kusumi, M. Mitsumata, K. Uchida, A lipid peroxidation-derived inflammatory mediator: identification of 4-hydroxy-2-nonenal as a potential inducer of cyclooxygenase-2 in macrophages, J. Biol. Chem. 279 (2004) 48389–48396.
[70] N. Harju, Regulation of oxidative stress and inflammatory responses in human retinal pigment epithelial cells, Acta Ophthalmol. 100 (Suppl 273) (2022) 3–59.
[71] Y.K. Cho, D.H. Park, I.C. Jeon, Medication trends for age-related macular degeneration, Int. J. Mol. Sci. 22 (2021).
[72] C.L. Cubitt, Q. Tang, C.A. Monteiro, R.N. Lausch, J.E. Oakes, IL-8 gene expression in cultures of human corneal epithelial cells and keratocytes, Invest. Ophthalmol. Vis. Sci. 34 (1993) 3199–3206.